



Publish with us
Submit an article

About this journal

Explore
Browse all articles & issues

Latest issue

Subscribe
Alerts & RSS feed

Ready to submit?

Start a new manuscript submission
or continue a submission in
progress

[Go to submission site](#)

Submission information

[Instructions for authors](#)

[Editorial policies](#)

Editing services

[Editing services site](#)

About this journal

[Journal metrics](#)

[Aims & scope](#)

[Journal information](#)

Journal information

Print ISSN: 1544-0478 Online ISSN: 1544-046X

12 issues per year

Journal of Natural Fibers is abstracted and indexed by the following services: CABI (listed in various services in CABI); EBSCOhost (listed in various services in EBSCOhost); Elsevier BV (Compendex, Scopus); TEMA - Technology and Management; OCLC (ArticleFirst, Electronic Collections Online); Ovid (Inspec); ProQuest (listed in various services in ProQuest); Thomson Reuters (Science Citation Index Expanded, Web of Science); VINITI RAN (Referativnyi Zhurnal); World Ceramics Abstracts

Taylor & Francis make every effort to ensure the accuracy of all the information (the "Content") contained in our publications. However, Taylor & Francis, our agents (including the editor, any member of the editorial team or editorial board, and any guest editors), and our licensors make no representations or warranties whatsoever as to the accuracy, completeness, or suitability for any purpose of the Content. Any opinions and views expressed in this publication are the opinions and views of the authors, and are not the views of or endorsed by Taylor & Francis. The accuracy of the Content should not be relied upon and should be independently verified with primary sources of information. Taylor & Francis shall not be liable for any losses, actions, claims, proceedings, demands, costs, expenses, damages, and other liabilities whatsoever or howsoever caused arising directly or indirectly in connection with, in relation to, or arising out of the use of the Content. Terms & Conditions of access and use can be found at



Low-Velocity Impact, Free-Fall Drop Test of Prototype, and Failure Analysis of Hybrid Palm / Kenaf Reinforced MWCNT Phenolic Composites

Tamil Moli Loganathan, Mohamed Thariq Hameed Sultan, Siti Madiha Muhammad Amir, Jesuarockiam Naveen, Mohamad Rabaie Shari, Shazana Mustapa, Mohamad Firdaus Saharudin, Irwan Shah B. Mohd Rabu, Ain Umaira Md Shah & Shukri Mohd

To cite this article: Tamil Moli Loganathan, Mohamed Thariq Hameed Sultan, Siti Madiha Muhammad Amir, Jesuarockiam Naveen, Mohamad Rabaie Shari, Shazana Mustapa, Mohamad Firdaus Saharudin, Irwan Shah B. Mohd Rabu, Ain Umaira Md Shah & Shukri Mohd (2022): Low-Velocity Impact, Free-Fall Drop Test of Prototype, and Failure Analysis of Hybrid Palm / Kenaf Reinforced MWCNT Phenolic Composites, Journal of Natural Fibers, DOI: [10.1080/15440478.2022.2133049](https://doi.org/10.1080/15440478.2022.2133049)

To link to this article: <https://doi.org/10.1080/15440478.2022.2133049>



Published online: 24 Oct 2022.



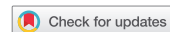
Submit your article to this journal [↗](#)



View related articles [↗](#)



View Crossmark data [↗](#)



Low-Velocity Impact, Free-Fall Drop Test of Prototype, and Failure Analysis of Hybrid Palm / Kenaf Reinforced MWCNT Phenolic Composites

Tamil Moli Loganathan^{a,b}, Mohamed Thariq Hameed Sultan^{a,c,d}, Siti Madiha Muhammad Amir^e, Jesuarockiam Naveen^f, Mohamad Rabaia Shari^e, Shazana Mustapa^g, Mohamad Firdaus Saharudin^g, Irwan Shah B. Mohd Rabu^h, Ain Umaira Md Shahⁱ, and Shukri Mohd^e

^aDepartment of Aerospace Engineering, Faculty of Engineering, Universiti Putra Malaysia, Serdang, Selangor, Darul Ehsan, Malaysia; ^bDepartment of Mechanical Engineering, Politeknik Banting Selangor, Banting, Selangor; ^cLaboratory of Biocomposite Technology, Institute of Tropical Forestry and Forest Products (INTROP), Universiti Putra Malaysia, Serdang, Selangor, Darul Ehsan, Malaysia; ^dPrime Minister's Department, Aerospace Malaysia Innovation Centre (944751-A), Cyberjaya, Selangor, Darul Ehsan, Malaysia; ^eIndustrial Technology Division, Malaysian Nuclear Agency, Bangi, Selangor, Malaysia; ^fSchool of Mechanical Engineering, Vellore Institute of Technology, Vellore, India; ^gDepartment of Aircraft Maintenance, Politeknik Banting Selangor, Banting, Selangor, Malaysia; ^hNDT Department, Composites Technology City, Melaka, Batu Berendam, Malaysia

ABSTRACT

The research's aim is to investigate the energy absorption, free-fall drop analysis, and failure analysis of Palm (P)/kenaf (K) fiber-reinforced MWCNT-phenolic composites. 3P:7K reinforced MWCNT-phenolic composites were made using manual mixing and hot pressing at 150°C with a pressure of 10 tonnes. Energy absorption was investigated using a drop weight impact tester. Free-fall drop test was performed to analyze the performance of the aircraft tray table prototype. Non-destructive testing was carried out to investigate the damage mechanism. The results demonstrate that as the impact energy increased from 1.50 J to 3.0 J, the crack length increased. There is a difference of 3% to 15% in the crack sizing between dye penetration and Digital Detector Array (DDA), indicating that DDA is more accurate. In the free-fall drop test, small cracks were detected in the dye penetration method on the prototype. The DDA approach, however, did not reveal any defects. The agglomerations were observed through DDA and Computed tomography. In this study, the hybrid CR/kenaf reinforced MWCNT modified phenolic composites exhibit superior performance that can act as an efficient and eco-friendly material for aircraft tray table application by preserving natural resources.

摘要

本研究旨在研究棕榈 (P) /红麻 (K) 纤维增强MWCNT酚醛复合材料的能量吸收、自由下落分析和失效分析。3P:7K增强MWCNT-酚醛复合材料是在150°C、10吨压力下通过手动混合和热压制成的。用落锤冲击试验机研究了能量吸收。进行自由跌落试验,以分析飞机托盘台原型的性能。为了研究损伤机理,进行了无损检测。结果表明,随着冲击能量从1.50 J增加到3.0 J,裂纹长度增加。染料渗透和数字探测器阵列 (DDA) 之间的裂纹尺寸差异为3%至15%,表明DDA更准确。在自由跌落试验中,在原型上的染料渗透法中检测到小裂纹。然而,DDA方法没有发现任何缺陷。通过DDA和计算机断层扫描观察结块。在本研究中,CR/红麻混杂增强MWCNT改性酚醛复合材料表现出优异的性能,通过保护自然资源,可作为飞机托盘桌应用的高效环保材料。

KEYWORDS

Hybrid composites; palm fiber; kenaf fiber; multi-walled carbon nanotubes; low-velocity impact; free-fall drop analysis; nondestructive testing

关键词

混杂复合材料; 棕榈纤维; 红麻纤维; 多壁碳纳米管; 低速冲击; 自由落差分析; 无损检测

Introduction

Composite structures are susceptible to catastrophic damages caused by impacts. The impact scenario can be classified into two types: 1) an object falling on the composite structure, and 2) the composite product itself falls (Hamamousse et al. 2019). Impact damage, particularly low-velocity impact, is widely recognized as one of the most critical threats to composite structures (Bensadoun et al. 2017). Therefore, during the design process, a deep understanding of the impact properties of composite structure is essential. The impact properties of a composite structure are influenced by several factors such as the fiber properties and its architecture, matrix type, specimen thickness, and projectile velocity (Bensadoun et al. 2017; Safri et al. 2014). Low-velocity impact properties are crucial for the interior components of aircrafts, especially tray tables. A low-velocity impact on a tray table refers to damages caused by events such as an object being dropped on the tray table whilst in use, or a hand tool being dropped during maintenance work (31 m/s) (Razali, Sultan, and Jawaid 2017). A free-fall drop test is closer to a “real” impact scenario on the composite structure. A free fall happens when an object is subjected to a pure gravitational acceleration. In the case of an aircraft tray table, it may fall during repair and replacement work. Therefore, it is imperative to conduct a free-fall drop test to determine the impact in an actual situation.

Instantaneous loads added to a surface during an impact incident may result in unexpected damages and can sometimes lead to structural failure. This is much worse when low-velocity impacts and free-fall incidents produce invisible damages; the cumulative damages from multiple repetitive accidents will contribute to catastrophic failures (Hamamousse et al. 2019). When exposed to impact loading, different mechanisms of damage initiation may be detected, and these findings demonstrate the dissipation of energy from the impact force to the composite structure. As a consequence, the tray table can be exposed to a low-velocity impact when an item drops on it, or due to a free-fall impact effect, which may lead to the creation of invisible defects that cause the tray table to collapse. Low-velocity impacts and free-fall damages are potentially dangerous and can lead to serious damage propagation (Ismail et al. 2019b).

Therefore, the impacted samples are inspected using a nondestructive testing (NDT) method as a post-inspection test. A variety of NDT techniques for the post-impact damage, such as visual inspection (Jiang et al. 2021), dye penetration (Zhang, Rao, and Li 2020), X-ray tomography (Cao et al. 2019), and computer tomography (Crupi et al. 2014), provide detailed information regarding the damage induced by LVI and free-fall drop tests. Visual inspection is a practice of visually inspecting the failed object to analyze the surface damage. Dye penetrant inspection is a commonly employed and an inexpensive method for detecting surface-breaking defects in non-porous materials. Digital Detector Array (DDA) is one of the better options to replace industrial films as it can view an image directly without a computer to analyze it (Moreira et al. 2010). X-ray computed tomography (CT) could detect any indication at a higher resolution at gauge planar. CT systems generate a three-dimensional image by taking several image “slices” at various angles along a single object rotation axis (Swoger et al. 2007).

Adequate awareness of sustainable materials and eco-legislation have driven researchers to find potential sustainable and green composites for synthetic fiber reinforced with polymer composites in the aerospace industry. Natural fibers provide distinct advantages over synthetic fibers, including renewability, sustainability, low environmental effects, large supply, light-weight, low cost, low carbon footprint, and mitigating environmental pollution. These features demonstrate the potential of natural fibers to offer adequate reinforcement in polymer composites. Kenaf bast fiber was chosen for its high tensile strength, while palm fiber was chosen for its high toughness; these characteristics compensate for each quality of the bio-composite (Loganathan et al., 2021b). Furthermore, natural fibers exhibit remarkable sound absorption properties and are viable substitutes for synthetic sound absorbers (Samaei et al. 2021). When kenaf is hybridized with palm fiber reinforcement, the bio-flexural composite’s stability improves.

According to earlier study, combination of palm and kenaf fiber compensate for each other in tensile and impact qualities to improve the mechanical properties of a hybrid composite. In a previous

study, the hybridization effects of Palm (P)/Kenaf (K) fiber-reinforced MWCNT phenolic composites in terms of mechanical and flammability properties were studied with variable ratios (Loganathan et al. 2021a). A composite of 3P:7K ratio was selected as an optimal hybrid composite based on TOPSIS method and proposed to be used as an interior component (for non-load bearing structures) in the aviation industry (Loganathan et al. 2021). The TGA, DTG, and DSC results from a previous study revealed that the composite of 3P:3K ratio had the best thermal stability compared to other hybrid composites evaluated. The hybrid composites of 3P:3K ratio produced smoke with a density less than 200, which satisfies the standards of the Federal Aviation Regulations (FAR) 25.853d, indicating that it could be potentially used in aviation or automobiles. In addition, phenolic derived from cashew nut shell liquid (CNSL) was selected to improve biodegradability.

Many studies have been executed by experts all over the world to expand the usage of natural fiber as a substitute for synthetic fiber in the aviation industry. The present work is the continuation of our previous study on the mechanical properties of palm/kenaf-reinforced MWCNT modified phenolic composites (Loganathan; *et al.* 2021). The optimal hybridization properties were chosen with a palm (P) kenaf (K) ratio of 3P:7K for the fabrication of an aircraft tray table prototype to study the impact properties. In the present study, a low-velocity impact and free-fall test on the prototype tray table was performed. Damage progressions of palm/kenaf-reinforced MWCNT modified phenolic composites of LVI samples and tray table was investigated using NDT methods such as visual inspection, dye penetration, digital detector array radiography, and computed tomography.

Materials and methods

Experimental design: materials and composite fabrication

The physical and mechanical properties of palm and kenaf are shown in Table 1. Sodium hydroxide (NaOH) pellet with a molecular weight of 40 g/mol and a density of 2.13 g/cm³ was purchased from R&M Chemicals. Meanwhile, P fiber was collected from Telok Panglima Garang Malaysia plantation and extracted manually from the leaf stalk by retting process. K and MWCNT were purchased from ZKK Sdn Bhd, Malaysia. MWCNT was synthesized using a chemical vapor deposition (CVD) technique consisting of 8–15 nanotube layers with a diameter and size ranged between 12–15 nm and 3–15 μm, respectively, with a purity of 97%. Chemovate Girinagar in Bangalore, India, supplied the phenolic resin (Novolac type) derived from CNSL mixed with a 10% hexamine hardener.

Preparation of Palm and Kenaf fiber

Dry P and K fibers were grinded until pulverized and sieved with a size of <0.3 mm using a sieve shaker machine. The fibers were then immersed distinctly in NaOH solution at a concentration of 3 wt% for an hour. Then, they were washed several times with distilled water to eradicate the residue and dried for 24 h in an oven with a temperature of 80°C.

Fabrication of composites

MWCNT of 0.5 wt% was added to the phenolic resin and dry-mixed using a ball milling for 25 h to produce a homogeneous distribution. The hybrid composites of 15 wt% of CR and 35 wt% of kenaf

Table 1. Physical and mechanical properties of palm and kenaf fiber.

Properties	Palm	Kenaf (Hanan, Jawaid, and Tahir 2018)
Density (g/cm ³)	1.4	1.5
Tensile strength (MPa)	119	223–930
Tensile Modulus (GPa)	1.5	11–53
Elongation at break (%)	3.13	1.6–10
Cellulose (%)	45.42	31–39
Hemicellulose (%)	18.97	8–13
Lignin	20.70	12.1

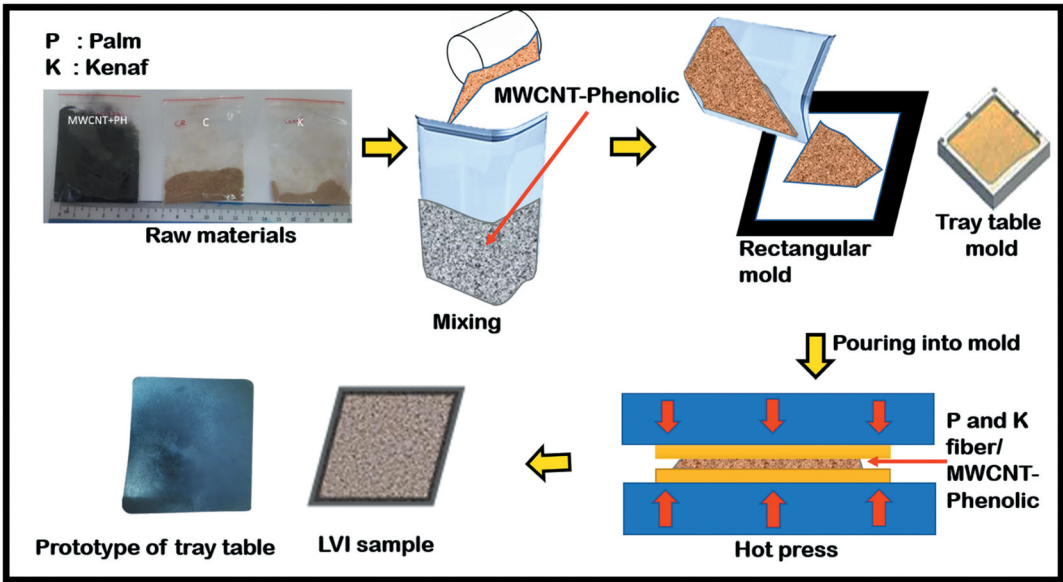


Figure 1. Schematic diagram of hybrid composite preparation for LVI and prototype of tray table.

were produced using a manual mixing technique with a mold size of 150 mm × 100 mm × 3 mm. The fiber was uniformly mixed manually with 0.5 wt% MWCNT–phenolic resin for 15 min. The mixture was then adequately spread into the mold. The mold was placed in a hot press with a temperature of 150°C and pressure of 10 tonnes, as illustrated in Figure 1. The composites were compressed for 10 min and were cold-pressed for 5 min.

Low-velocity impact testing

Drop-weight impact testing was performed to investigate low-velocity impact behavior of the hybrid bio-composites. The testing was performed with three repeatability samples on an instrumented drop weight impact tester model, IMATEK IM10, in accordance with ASTM D7136 as shown in Figure 1. The instrument was equipped with a data acquisition system, which records power, time, displacement, velocity, and energy absorbed by the samples being measured. Specimens with dimensions of 150 mm × 100 mm × 3 mm were clamped using rubber tip toggle clamps at four points with an equal clamp force in the impact support fixture with a cutout rectangular opening. A hemispherical tip striker with a radius of 5 mm and a weight of 5.101 kg was dropped onto the clamped composite sample from a calculated height. The impact energy added to the samples varied from 1.5 J to 3.0 J, and various heights were used to reflect different magnitudes. The impact energy, E , was measured using Equation (1) below:

$$EI = mgh \quad (1)$$

where m is the impactor mass, g is the gravitational acceleration (9.81 m/s²), and h is the height of the impactor.

Free-fall drop test

A drop tester machine for free-fall drop tests an object that can be dropped freely from a certain altitude to determine the capability of the object to withstand the sudden shock of a free fall. The prototype of an aircraft tray table was tested for free-fall drop at a maximum height of 130 cm in horizontal and vertical positions with three repetitions, respectively, using an air-arm-type drop, model KD-128A, manufactured by King Design Industrial Co-Ltd, Taiwan. The free-fall drop test was performed in compliance with ASTM D5276, as shown in Figure 2. The drop tester instrument was equipped with a data acquisition system for data analysis. The benefit of this testing is that the object falls spontaneously, resulting in a more realistic drop testing.

Post-impact damage by nondestructive testing

Visual inspection

Visual inspections were performed on the low-velocity samples and prototype after mechanical tests. These inspections were conducted in compliance with BS EN 13018:2001 to look for signs of defects such as noticeable cracks, structural defects, or other physical defects. Visual inspection was performed using a digital inspection camera.

Dye penetration

Liquid penetration inspection is the most effective and convenient method to inspect defects on the surface. The method relies on a liquid's ability to be drawn into a "clean" surface breaking flaw by

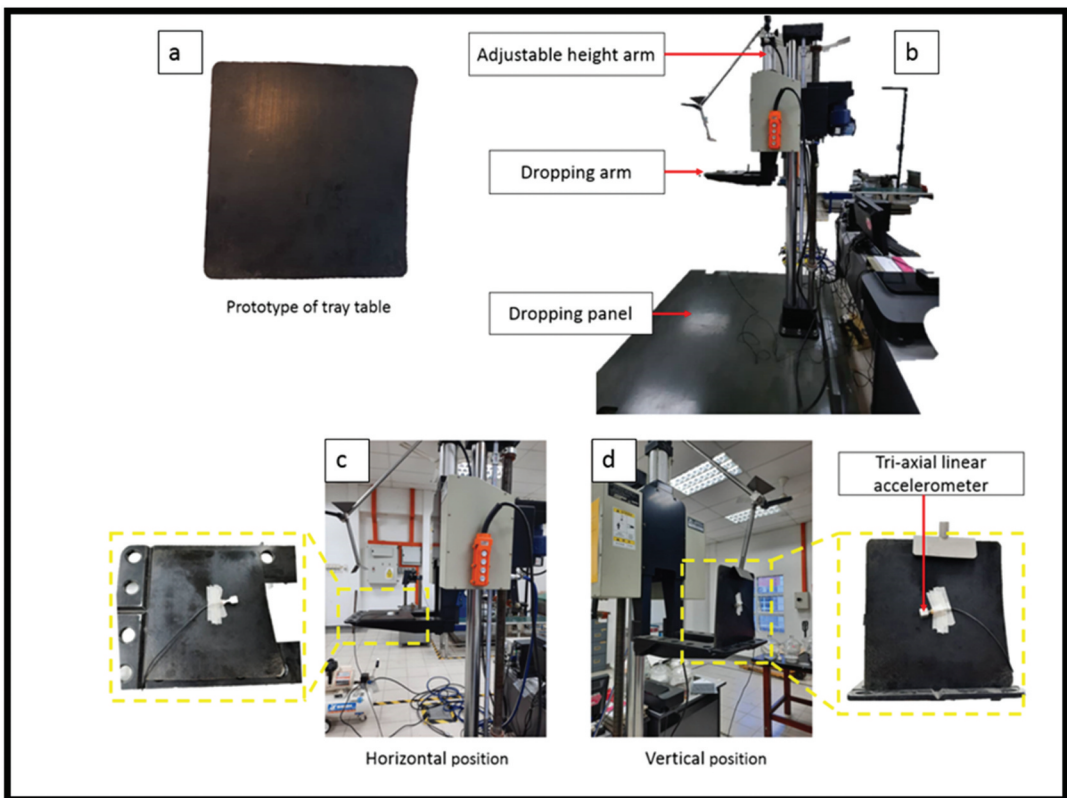


Figure 2. (a) Prototype of tray table, (b) Free-fall drop tester, (c) Prototype dropped in horizontal position and d) vertical position.

capillary action. Liquid penetration inspection was performed on the low-velocity impact samples and prototype of tray table as a posttest in order to indicate and identify cracks, impact fractures, and matrix failure. This testing was carried out in accordance with ASTM E1417. This process involved six stages, which were (1) pre-cleaning, (2) application of penetrant, (3) removal of excessive penetrant, (4) application of developer, (5) inspection of test surface, and (6) post-inspection cleaning, as shown in Figure 3. In the pre-cleaning stage, the composite surface was sprayed with solvents and allowed to dry to prevent any soil, paint, oil, or grease. The fluorescent penetration was then applied on the composite surface. It took approximately 20 min for the penetrant to “dwell” in any defects on the surface. The residual penetrant was then wiped away from the surface with a lint-free cloth. Residual penetrant was removed in one direction, either vertically or horizontally. A developer was applied to the sample after the excess penetrant was removed. For fluorescent penetrant examinations, sufficient ultraviolet (UV-A) radiation ($1,000 \text{ uW/cm}^2$) as well as low ambient light levels (less than 20 lux) were required. The post-inspection process was done with solvents on the inspected composites.

Digital Detector Array (DDA) radiography

The DDA was fixed on one side of the specimen, and an X-ray tube (source) was located on the other side. The DDA was tested on the LVI samples and on the prototype of tray table after the free-fall drop test. The measurements were made with an X-ray tube with a focal spot size of 3.0 mm and a maximum high voltage of 150 kV, a current of 1.0 mA, an integration time of 8 s, and a distance of 700 mm between the X-ray source and the DDA. The tests were performed in accordance with ASTM E2736. The X-ray radiation was directed onto the specimen, and the transmitted intensity across the specimen was captured on DDA. A defect or irregularity in the specimen will retain the radiation more or less, depending on its density in relation to the matrix, which will be visible in photographs with correlated contrast at various gray levels.

Computed Tomography (CT) scan

X-rays are used in computed tomography (CT) to produce 3D cross-sectional images as a volumetric representation. The impact damage of the LVI test and the free-fall drop test were studied in this work using an X-ray Computed Tomography System model XYLON, MGC 41 as shown in Figure 4. The focal spot size, source detector distance (SDD), and source object distance (SOD) for the LVI samples were set to 1 mm, 1000 mm, and 400 mm, respectively, with a maximum voltage of 30 kV and current of 2.0 mA. Meanwhile, for the prototype of tray table, the focal spot size, SDD, and SOD were set to 1 mm, 1000 mm, and 500 mm, respectively, with maximum voltage of 50 kV and current of 3.0 mA. The tests were conducted in accordance with ASTM E1441. The Linear Array Detector (LAD) detector system was used with a resolution of 0.4 mm/pixel. The sonogram images acquired from the CT-scan were created using Octopus tools.

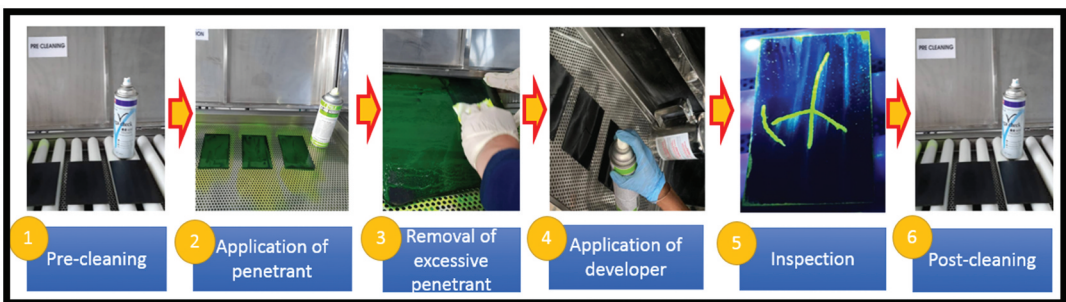


Figure 3. Procedure of dye penetration testing.

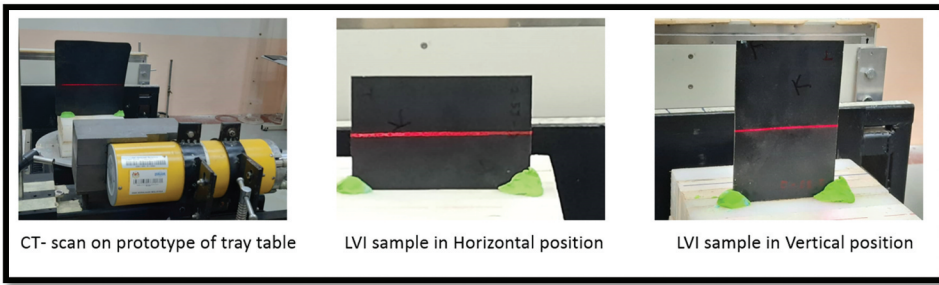


Figure 4. CT scanning.

Results and discussion

Low-velocity impact

Figure 5 displays the force–displacement curve of 3P:7K hybrid composites, with the impact energy level varying from 1.5 J to 3.0 J. In general, three stages of deformation are associated with the drop test distortion, which are (1) stopping and rebounding, (2) stopping but not rebounding, and (3) perforation (Ismail et al. 2019a, 2019b). The open curve in the graph below indicates that a perforation had occurred. The impactor's kinetic energy was transferred to the specimen and stored partially in the elastic deformation, with the remaining energy being dissipated as inertia, heat, and sound (Ismail et al. 2019a). The final energy value represents the cumulative energy dissipated by the specimen due to the occurrence of damage within the composites.

Table 2 presents the raw data obtained from the drop test data acquisition system. Referring to the data from Table 2 and Figure 5, it can be seen that the hybrid sample with a weight percentage ratio of 3P:7K, at an impact energy of 1.5 J, the absorbed energy reached 1.47 J, the peak force about 4.54 kN, peak deformation around 7.66 mm while peak deformation energy had reached up to 1.86 J. (Ismail et al. 2019) carried a low-velocity impact on hybrid composite-based woven flax and carbon fiber and discovered that the absorbed energy reached 3.31 J for 5 kN. This is virtually identical energy absorption for hybridization of natural–natural hybrid composite. Therefore, this hybrid palm/kenaf is comparable with hybridization of natural-synthetic fiber

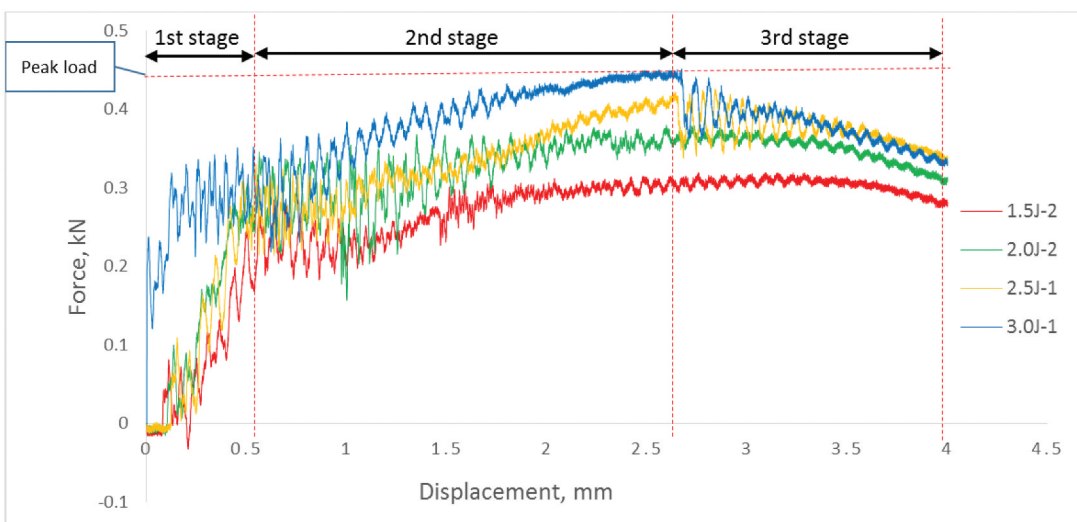


Figure 5. Force vs displacement curve of 3P:7K hybrid bio-composite.

Table 2. Data tabulation of low-velocity impact of 3P:7K hybrid bio-composite.

Joule	Height of sticker (m)	Peak force (kN)	Impact energy (J)	Peak deformation (mm)	Absorbed energy (J)	Energy to peak deformation (J)
1.5 J	0.03	0.32 (0.04)	1.47 (0.35)	7.66 (1.21)	1.86 (0.27)	1.86 (0.32)
2.0 J	0.04	0.38 (0.03)	1.99 (0.03)	8.18 (0.21)	2.36 (0.04)	2.40 (0.02)
2.5 J	0.05	0.43 (0.04)	2.46 (0.02)	9.82 (0.25)	2.93 (0.05)	2.95 (0.04)
3.0 J	0.06	0.45 (0.04)	2.99 (0.04)	10.42 (0.88)	3.55 (0.03)	3.61 (0.05)

() standard deviation.

and potential for replace synthetic fiber-based composite. When the impact energy was increased to 3.0 J, the absorbed energy, peak force, peak deformation, peak deformation energy, and impact energy increased by approximately 90%, 40%, 36%, 94%, and 103%, respectively, in comparison to the 1.5 J impact energy. This may be explained by the theory of energy conservation. Kinetic energy, alternatively referred to as the total energy prior to impact, equals the total energy after impact (Gliszczynski 2018). The deformation within the specimen is induced by the impactor's kinetic energy. The damage propagation within the specimen is proportional to the amount of energy absorbed by the specimen (Ismail et al. 2019a). An increase in the incident energy results in increased energy absorption by the specimen, which leads to more severe damage incurred within.

Figure 6 represents the energy curve against time of 3P:7K hybrid bio-composites. The absorbed energy is the energy absorbed by the specimen as a result of damage development and friction between the impactor and the specimen. The absorbed energy can be obtained from the curve of energy over time (Vaidya 2011), which indicates that the energy level becomes constant over a period. As seen in Figure 8, the absorbed energy increased as the incident impact energy increased. At the perforation impact stage (third stage), the impactor's energy was adequate to pierce the specimen. As a result, there was no decrease in the energy absorption curve, and the specimen dissipated the majority of the absorbed energy through damage propagation. The fiber length has a considerable effect on energy absorption since fiber acts as a load transfer medium. The longer fibers prevent crack propagation, and the shear force generated between them finally improves the impact strength. Additionally, Amuthakkannan et al. (2013) discovered that the length of the fiber had a major effect on the strength of the impact, and that when the energy impact exceeded the fiber strength, the fiber fractured.

As a result, the longer fibers resist crack development, and the shear force generated between them gradually increases the amount of energy absorbed.

Free-fall drop test

The free-fall drop test motions of the prototype were recorded using a tri-axial linear accelerometer. The test results were composed using King Design software, which provides scientific and digital data analysis of the free-fall drop testing on the tray table prototype. Prior to the testing, the weight of the tray table was measured and the environment data were entered in the King Design software.

The acceleration of free-falling objects is referred to as gravity acceleration. Figure 7 shows the curve of gravitational acceleration versus time, in the direction of X, Y, and Z axes, when the tray table was dropped from an altitude of 130 cm. Based on the graph, the gravitational acceleration versus time can be divided into four modes: static, free fall, impact, and steady states. The steady state is where the tray table was dropped from the dropping arm and fell down in 26 ms. The length of each mode for the

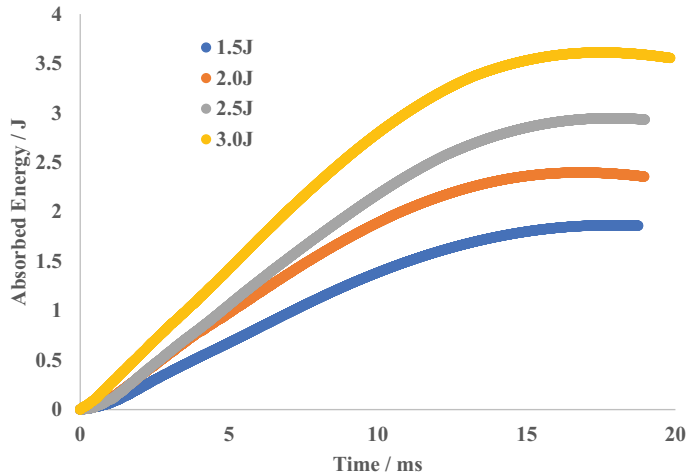


Figure 6. Energy vs time curve of 3P:7K hybrid bio-composites.

horizontal and vertical positions were almost identical; however, the impact mode for the horizontal position was found to be longer. When the tray table fell vertically, it returned to the steady state more quickly than when it fell horizontally.

As shown in Figure 8, the free-fall drop test principle is related to energy conversion, in which gravitational potential energy at rest is converted to kinetic energy. Even when the vertical and horizontal positions of the dropping arm maintained the same altitude, the exact height of each position varied significantly. The exact height was calculated from the datum to the center of gravity of the tray table. Therefore, the potential energy of the tray table in a vertical position was slightly higher compared to a horizontal position. In the vertical position, the impact duration is shorter compared to the horizontal position, thus sudden impact may lead to severe damage. During the maintenance of the tray table when it falls in the horizontal position, the damage will be lesser compared to vertical position.

Table 3 displays a triaxial linear accelerometer for the horizontal and vertical positions of the tray table. The velocity is the speed at which the object is traveling right before it makes contact with the ground (Vicovaro 2014). The tray table is no longer in free-fall until it touches the ground. It shows that the acceleration of the tray table in a horizontal position was higher than the vertical position. This may be due to the shorter traveling time of the horizontal tray table. In addition, the air resistance for the vertical position of the tray table was higher compared to the horizontal position.

Post-impact damage by nondestructive testing

Visual inspection

Table 3 illustrates the results of visual inspection, dye penetration, DDA, and CT-scan. From the visual inspection of the LVI samples, it was noticed that matrix cracks are visible. Due to the brittle nature of the phenolic matrix, matrix cracks can form during LVI. This is also supported by (Gaudenzi et al. 2015; Richardson and Wisheart 1996) that thermoset composite materials are brittle and that the majority of energy is absorbed via damage mechanisms rather than elastic deformation. When the impactor struck the top surface of the specimen during the LVI test, the surface crack propagated all the way to the bottom surface. The crack was initiated at the indentation spot. Weaver et al. found that when a crack approaches the impact surface, an elastic modulus mismatch occurs, which can be deflected at the interface or propagated across the stiffer area (Weaver et al. 2012). It is also noticed that the cracks on the back surface were more severe than the front surface. The crack pattern varies depending on the energy level. The higher the impact energy, the more severe the cracks are



Figure 7. Gravitational acceleration versus time at a) horizontal position and b) vertical position.

propagated in the specimens. From the visual inspection on the prototype of the tray table, no defects were observed after the free-fall drop test as presented in [Table 4](#).

Dye penetration and DDA

[Table 5](#) tabulates the dye penetration and DDA results. As seen in [Table 5](#), matrix cracking was observed on the composite samples, with impact energy levels ranging from 1.5 J to 2.0 J, 2.5 J, and 3.0 J. It was found that the matrix cracking propagated from the top to the bottom of the rectangular plates and from the middle (indentation) to the outer edges. The matrix crack propagation was halted until it reached the sides of the materials, preserving the rectangular shape of the sample without perforation. The use of micro-sized fibers with a random orientation limited the damage studied. Hence, no pattern can be proposed about the association of the impact energy levels with the magnitude of the damage incurred (Shah, Sultan, and Safri 2020; Živković et al. 2017).

Even though no pattern of the matrix crack propagation can be discerned, the study provides the crack propagation size between the center and the sides of the rectangular samples. Loganathan et al. reported that the impact strength of phenolic composites decreased significantly as the length of the

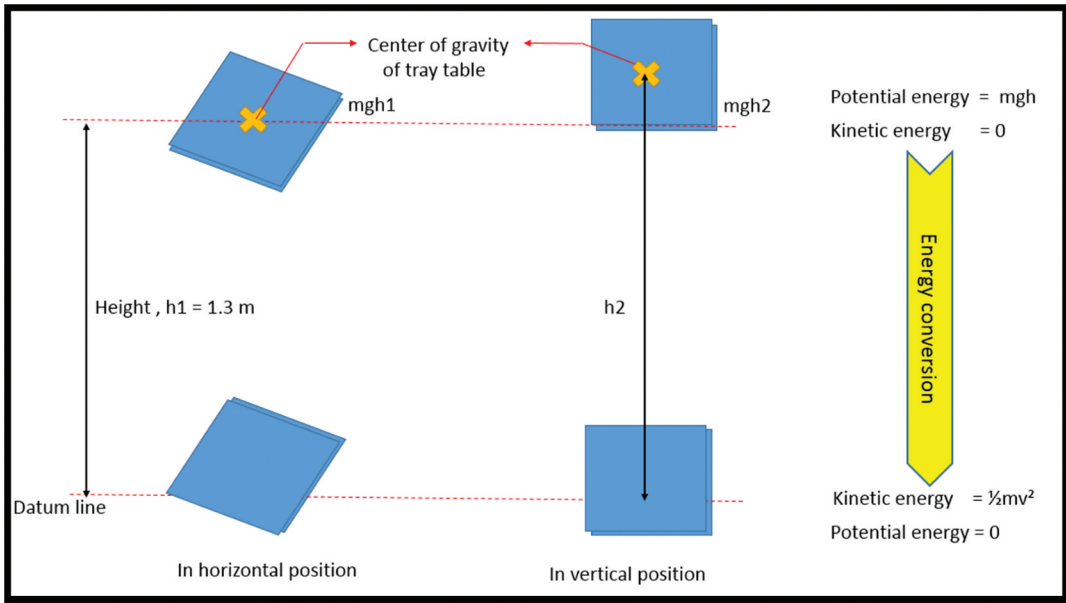


Figure 8. Energy conversion.

Table 3. A triaxial linear accelerometer for a) horizontal and b) vertical positions of tray table.

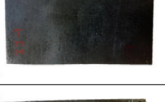
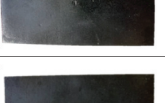
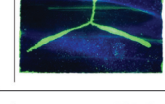
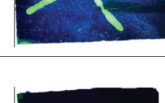
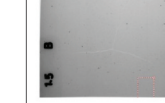
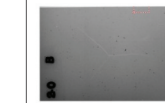
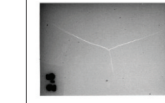
Position of tray table	Axis	Acceleration, (G's)	Time, (mS)	Velocity, (m/S)	Maximum Acceleration, G's	Minimum Acceleration, G's
Horizontal	X	13.67 ± 1.44	2.87 ± 1.37	0.15 ± 0.04	13.67 ± 1.44	-2.25 ± 1.09
	Y	144.38 ± 2.68	2.91 ± 1.71	1.75 ± 0.93	144.48 ± 2.61	-108.97 ± 1.09
	Z	328.15 ± 33.51	1.21 ± 0.27	1.88 ± 0.22	328.15 ± 33.51	-116.81 ± 25.34
Vertical	X	9.64 ± 1.92	3.69 ± 0.29	0.15 ± 0.01	9.64 ± 1.92	-2.22 ± 2.41
	Y	99.32 ± 12.64	6.20 ± 0.10	2.73 ± 0.58	99.32 ± 12.64	-72.67 ± 17.85
	Z	250.67 ± 26.11	1.29 ± 0.29	1.50 ± 0.06	250.67 ± 26.11	-166.57 ± 18.43

natural fiber was reduced (Loganathan et al. 2021). This can be due to the presence of a greater amount of hollow mortar brick structures in comparison to a fiber length of less than 0.3 mm, resulting in efficient energy absorption.

The length of the crack extended as the impact energy increased from 1.50 J to 3.0 J, as seen in Figure 9. This is supported by the fact that the damage area increases as the incident impact energy rises. A similar finding was reported by (Shah, Sultan, and Safri 2020), who carried out dye penetration on LVI samples made from bamboo-reinforced epoxy composites when the impact energy varied from 2.50 J, 3.75 J, and 4.40 J. The crack pattern in both tests was similar, and the size of defects were measured. A significant difference of approximately 3–15% in the defect sizing between both test results was found. If the dwell time was set to 15 min after developer application, this composite material would be erect to liquid and the crack would thicken, as shown in the 1.5 J and 2.0 J images (top). Therefore, the measurement of the crack length in dye penetration may have a small significant difference compared to the sizing made with the DDA results.

Predominantly, when the applied impact energy approaches the threshold value for penetrating the specimens, the possibility of fiber breakage increases. When the impact energy is sufficient to penetrate the specimen, the matrix cracks as a result of the shear stress. On the other hand, the matrix crack occurred during LVI due to the brittle nature of the phenolic composite.

Table 4. Results of NDT inspection on prototype of tray table.

Joule	Low velocity impact							
	1.5		2.0		2.5		3.0	
	Front	Back	Front	Back	Front	Back	Front	Back
Visual inspection								
Dye penetration								
DDA								

(Continued)

Table 4. (Continued).

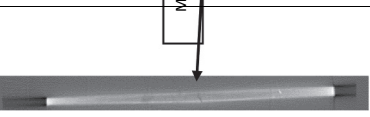
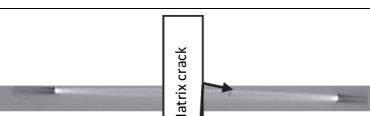
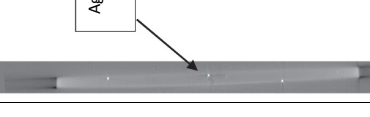
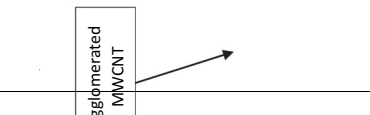
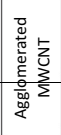
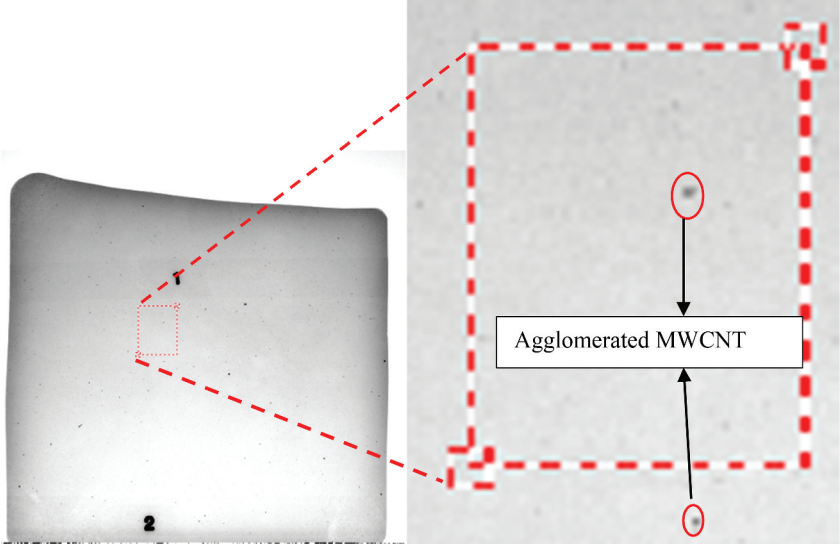
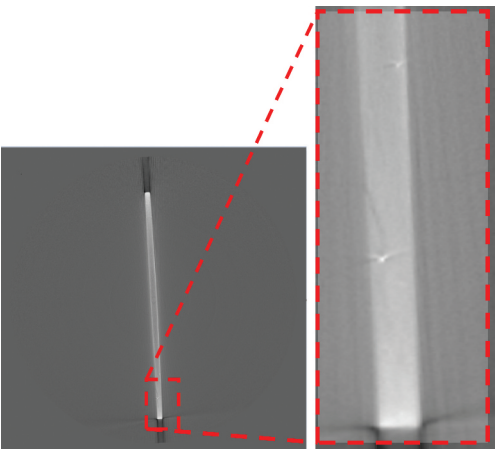
		Low velocity impact						
Joule	1.5		2.0		2.5		3.0	
	Front Horizontal	Back Vertical	Front Horizontal	Back Vertical	Front Horizontal	Back Vertical	Front Horizontal	Back Vertical
CT- scan								
								

Table 5. Results of NDT inspection on LVI specimens.

Types	Prototype tray table
Visual inspection	
Dye penetration	
DDA	

(Continued)

Table 5. (Continued).

Types	Prototype tray table
CT-scan	

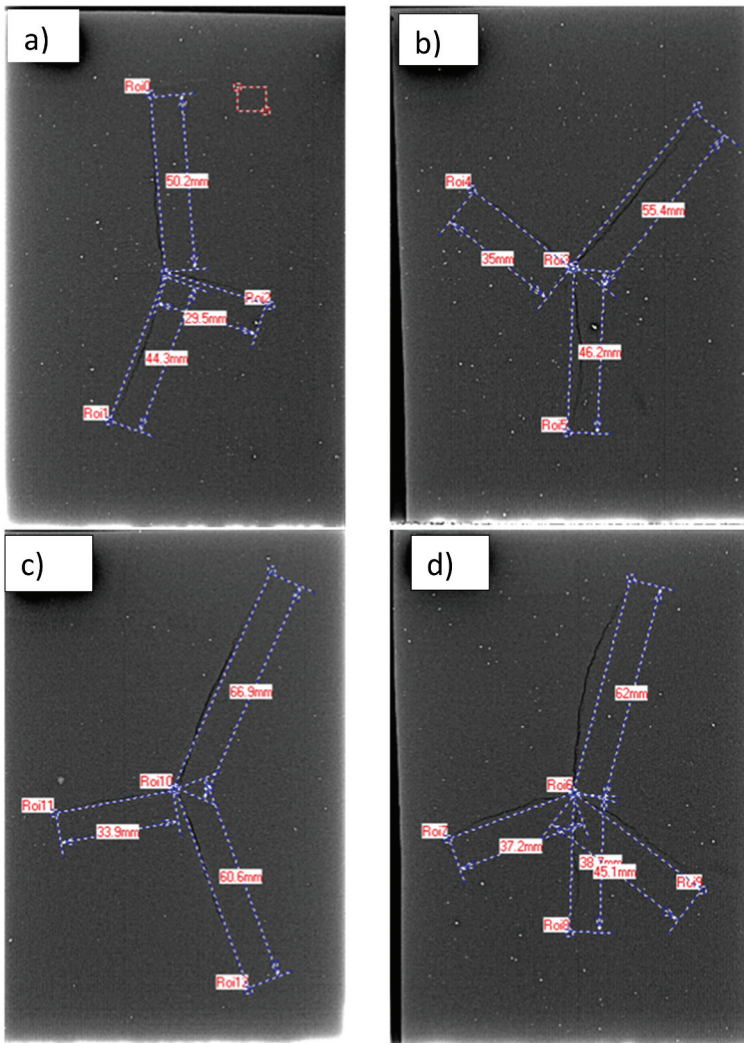


Figure 9. Sizing of the cracks from DDA images of (a) 1.5 J, (b) 2.0 J, (c) 2.5 J, and (d) 3.0 J.

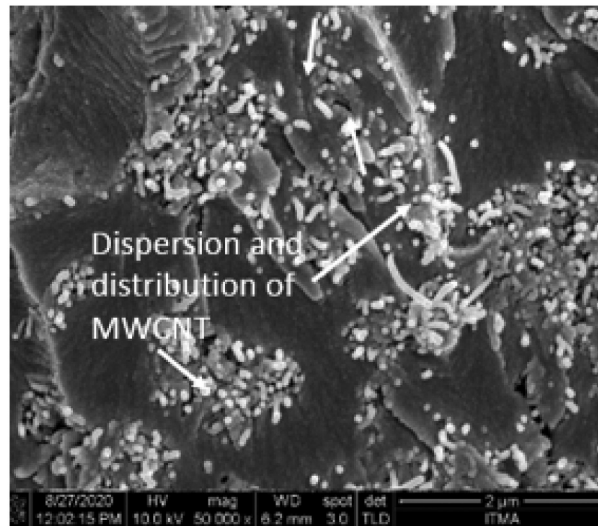


Figure 10. FE-SEM images of 3P:7K specimens at magnification of x50000 (Loganathan et al. 2021).

For the tray table after the free-fall drop test, some small cracks were observed using dye penetration method. However, the small cracks were not visible using the DDA method. According to the enlarged image of the DDA, dark spots were observed. This indicates the agglomeration of MWCNT. According to Aguilar et al., the agglomerated condition is described by an increase in the density of CNT-to-CNT junctions after the percolating network has developed (Aguilar, Bautista-Quijano, and Avilés 2010). Based on the density difference, the darker area implies more exposure with higher radiation level, while the lighter region indicates lesser exposure. According to a previous research, the FE-SEM photographs of MWCNT agglomeration in phenolic composites shown in Figure 10 demonstrate the MWCNT dispersion and that distribution is uneven and challenging to control (Ma et al. 2010).

CT-Scan

In the CT-scan method, the cross sections of the horizontal and vertical positions of the LVI samples' defect were investigated. As seen in Figure 4, the CT-scan was used to analyze the cross section of the composite plate around the damaged area's middle (indentation). The crack was observed at several locations along the cross-sectional view for the all the samples with various impact energy levels. The images illustrate that none of the samples had undergone perforation. The first form of failure is matrix cracking, which occurred as a result of the low-velocity impact effect caused by tension, compression, and shearing. Matrix cracking can be classified into two types: shear cracking (inclination of 45°) and bending crack (vertical inclination) (Safri et al. 2014). The bending crack propagated until the matrix cracked. The white dots in the images are agglomerated MWCNT, similar to the DDA. The agglomerated MWCNT acts as a stress concentrator, which leads to crack branching. A similar finding was reported by Shokrieh et al. who found that a large agglomeration of nanotubes as a stress concentrator causes the sample to fail at lower stresses (Shokrieh, Saeedi, and Chitsazzadeh 2013). The CT-scan for the tray table demonstrated that a small crack was found exactly at the agglomeration of MWCNT. As mentioned previously, an agglomeration of MWCNT in the phenolic acts as a stress concentrator and weakens the region as illustrated in Figure 11.

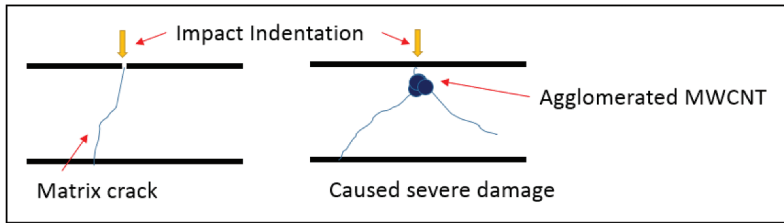


Figure 11. Crack propagation during impact energy on composite sample.

Conclusions

The low-velocity impact behavior and free-fall drop test of a tray table prototype made of hybrid Palm (P)/kenaf fiber (K) reinforced MWCNT modified phenolic composites at a 3P:7K reinforcement ratio were studied. The impact damage assessments for the LVI specimens and free-fall drop test of tray table prototype were performed using four methods: visual examination (photography images), dye penetration, DDA, and CT-scan method. The visual examination revealed cracks on the LVI samples; however, the dye penetration and DDA methods revealed cracks and allowed for sizing of the LVI samples. For the tray table inspection via DDA, no defects were observed as an indication because the small crack is presence not volumetric. An agglomerated MWCNT can be detected using DDA and CT-scan, but other methods are insensitive to it. In this study, a hybrid palm/kenaf reinforced MWCNT modified phenolic composite is proposed for aircraft interior componenttr as an eco-friendly material by preserving natural resources. The proposed bio-composite has shown excellent resistance to the impact load; hence, it can be used for tray table application that is recyclable and biodegradable.

Highlights

- Energy absorption, free-fall drop analysis, and failure analysis of palm (P)/kenaf (K) fiber-reinforced MWCNT-phenolic composites were studied.
- Visual examination revealed cracks on the LVI samples.
- Dye penetration and DDA methods revealed cracks and allowed for sizing.
- An agglomerated MWCNT was detected using DDA and CT-scan.
- 3P:7K reinforced MWCNT–phenolic composites is proposed for aircraft tray table.

Acknowledgements

The authors would like to express their gratitude and sincere appreciation to the Department of Aerospace Engineering, Faculty of Engineering, Universiti Putra Malaysia and Laboratory of Biocomposite Technology, Institute of Tropical Forestry and Forest Products (INTROP), Universiti Putra Malaysia (HICOE) for the close collaboration in this research. The authors also extend their acknowledgment to Polytechnic Banting Selangor and Malaysian Nuclear Agency for their support in terms of the NDT testing.

Disclosure statement

No potential conflict of interest was reported by the author(s).

Funding

This work is supported by UPM under GPB grant, 9668200.

ORCID

Tamil Moli Loganathan  <http://orcid.org/0000-0001-6908-0457>

Ain Umaira Md Shah  <http://orcid.org/0000-0002-6957-4112>

References

- Aguilar, J., J. Bautista-Quijano, and F. Avilés. 2010. Influence of carbon nanotube clustering on the electrical conductivity of polymer composite films. *Express Polym Lett* 4 (5):292–99. doi:10.3144/expresspolymlett.2010.37.
- Amuthakkannan, P., V. Manikandan, J.W. Jappes, and M. Uthayakumar. 2013. Effect of fibre length and fibre content on mechanical properties of short basalt fibre reinforced polymer matrix composites. *Materials Physics and Mechanics* 16 (2):107–17. doi:10.1016/j.compositesb.2011.11.009.
- Bensadoun, F., D. Depuydt, J. Baets, I. Verpoest, and A. W. Van Vuure. 2017. Low velocity impact properties of flax composites. *Composite Structures* 176:933–44. doi:10.1016/j.compstruct.2017.05.005.
- Cao, W., J. Zhang, B. Sun, and B. Gu. 2019. X-ray tomography and numerical study on low-velocity impact damages of three-dimensional angle-interlock woven composites. *Composite Structures* 230:111525. doi:10.1016/j.compstruct.2019.111525.
- Crupi, V., G. Epasto, E. Guglielmino, H. Mozafari, and S. Najafian. 2014. Computed tomography-based reconstruction and finite element modelling of honeycomb sandwiches under low-velocity impacts. *Journal of Sandwich Structures & Materials* 16 (4):377–97. doi:10.1177/1099636214531515.
- Gaudenzi, P., D. Nardi, I. Chiappetta, S. Atek, L. Lampani, M. Pasquali, F. Sarasini, J. Tirilló, and T. Valente. 2015. Sparse sensing detection of impact-induced delaminations in composite laminates. *Composite Structures* 133:1209–19. doi:10.1016/j.compstruct.2015.08.052.
- Gliszczynski, A. 2018. Numerical and experimental investigations of the low velocity impact in GFRP plates. *Composites Part B: Engineering* 138:181–93. doi:10.1016/j.compositesb.2017.11.039.
- Hamamousse, K., Z. Sereir, R. Benzidane, F. Gehring, M. Gomina, and C. Poilâne. 2019. Experimental and numerical studies on the low-velocity impact response of orthogrid epoxy panels reinforced with short plant fibers. *Composite Structures* 211:469–80. doi:10.1016/j.compstruct.2019.01.005.
- Hanan, F., M. Jawaid, and P.M. Tahir. 2018. Mechanical performance of oil palm/kenaf fiber-reinforced epoxy-based bilayer hybrid composites. *Journal of Natural Fibers* 17 (2):155–67. doi:10.1080/15440478.2018.1477083.
- Ismail, M. F., M. T. Sultan, A. Hamdan, A. U. Shah, and M. Jawaid. 2019b. Low velocity impact behaviour and post-impact characteristics of kenaf/glass hybrid composites with various weight ratios. *Journal of Materials Research and Technology* 8 (3):2662–73. doi:10.1016/j.jmrt.2019.04.005.
- Ismail, K., M. Sultan, A. Shah, M. Jawaid, and S. Safri. 2019a. Low velocity impact and compression after impact properties of hybrid bio-composites modified with multi-walled carbon nanotubes. *Composites Part B: Engineering* 163:455–63. doi:10.1016/j.compositesb.2019.01.026.
- Jiang, F., G. Zhidong, L. Zengshan, and W. Xiaodong. 2021. A method of predicting visual detectability of low-velocity impact damage in composite structures based on logistic regression model. *Chinese Journal of Aeronautics* 34 (1):296–308. doi:10.1016/j.cja.2020.10.006.
- Loganathan, T. M., M. T. H. Sultan, Q. Ahsan, A. U. M. Shah, M. Jawaid, A. R. A. Talib, and A. A. Basri. 2021a. Physico-mechanical and flammability properties of cyrtostachys renda fibers reinforced phenolic resin bio-composites. *Journal of Polymers and the Environment* 29 (11):3703–20. doi:10.1007/s10924-021-02135-0.
- Loganathan, T. M., M. T. H. Sultan, M. Jawaid, Q. Ahsan, J. Naveen, A. U. M. Shah, A. R. A. Talib, and A. A. Basri. 2021b. Physical, mechanical, and morphological properties of hybrid cyrtostachys renda/Kenaf fiber reinforced with multi-walled carbon nanotubes (MWCNT)-phenolic composites. *Polymers* 13 (19):3448. doi:10.3390/polym13193448.
- Ma, P.-C., N. A. Siddiqui, G. Marom, and J.-K. Kim. 2010. Dispersion and functionalization of carbon nanotubes for polymer-based nanocomposites: A review. *Composites: Part A, Applied Science and Manufacturing* 41 (10):1345–67. doi:10.1016/j.compositesa.2010.07.003.
- Moreira, E., J. Barbosa Rabello, M. Pereira, R. Lopes, and U. Zscherpel. 2010. Digital radiography using digital detector arrays fulfills critical applications for offshore pipelines. *EURASIP Journal on Advances in Signal Processing* 2010 (1):894643. doi:10.1155/2010/894643.
- Razali, N., M. T. H. Sultan, and M. Jawaid. 2017. A review on detecting and characterizing damage mechanisms of synthetic and natural fiber based composites. *BioResources* 12 (4):9502–19. doi:10.15376/biores.12.4.Razali.

- Richardson, M., and M. Wisheart. 1996. Review of low-velocity impact properties of composite materials. *Composites: Part A, Applied Science and Manufacturing* 27 (12):1123–31. doi:10.1016/1359-835X(96)00074-7.
- Safri, S., M. Sultan, N. Yidris, and F. Mustapha. 2014. Low velocity and high velocity impact test on composite materials—a review. *International Journal of Engineering Science* 3 (9):50–60.
- Samaei, S. E., U. Berardi, P. Soltani, and E. Taban. 2021. Experimental and modeling investigation of the acoustic behavior of sustainable kenaf/yucca composites. *Applied Acoustics* 183:108332. doi:10.1016/j.apacoust.2021.108332.
- Shah, A. U. M., M. T. H. Sultan, and S. N. A. Safri. 2020. Experimental evaluation of low velocity impact properties and damage progression on bamboo/glass hybrid composites subjected to different impact energy levels. *Polymers* 12 (6):1288. doi:10.3390/polym12061288.
- Shokrieh, M. M., A. Saeedi, and M. Chitsazzadeh. 2013. Mechanical properties of multi-walled carbon nanotube/polyester nanocomposites. *Journal of Nanostructure in Chemistry* 3 (1):20. doi:10.1186/2193-8865-3-20.
- Swoger, J., P. Verveer, K. Greger, J. Huisken, and E. H. Stelzer. 2007. Multi-view image fusion improves resolution in three-dimensional microscopy. *Optics Express* 15 (13):8029–42. doi:10.1364/OE.15.008029.
- Vaidya, U. K. 2011. Impact response of laminated and sandwich composites. In Abrate, S. (eds), *Impact engineering of composite structures*, 97–191. Vienna: Springer.
- Vicovaro, M. 2014. Intuitive physics of free fall: An information integration approach to the mass-speed belief. *Psicológica* 35 (3):463–77.
- Weaver, J. C., G. W. Milliron, A. Miserez, K. Evans-Lutterodt, S. Herrera, I. Gallana, W. J. Mershon, B. Swanson, P. Zavattieri, and E. Dimasi. 2012. The stomatopod dactyl club: A formidable damage-tolerant biological hammer. *Science* 336 (6086):1275–80. doi:10.1126/science.1218764.
- Zhang, C., Y. Rao, and W. Li. 2020. Low-velocity impact behavior of intralayer hybrid composites based on carbon and glass non-crimp fabric. *Composite Structures* 234:111713. doi:10.1016/j.compstruct.2019.111713.
- Živković, I., C. Fragassa, A. Pavlović, and T. Brugo. 2017. Influence of moisture absorption on the impact properties of flax, basalt and hybrid flax/basalt fiber reinforced green composites. *Composites Part B: Engineering* 111:148–64. doi:10.1016/j.compositesb.2016.12.018.